

Journal of Photonics for Energy

SPIEDigitalLibrary.org/jpe

Formulation strategies for optimizing the morphology of polymeric bulk heterojunction organic solar cells: a brief review

Uyxing Vongsaysy
Dario M. Bassani
Laurent Servant
Bertrand Pavageau
Guillaume Wantz
Hany Aziz

Formulation strategies for optimizing the morphology of polymeric bulk heterojunction organic solar cells: a brief review

Uyxing Vongsaysy,^{a,b,c,*} Dario M. Bassani,^a Laurent Servant,^a
Bertrand Pavageau,^b Guillaume Wantz,^d and Hany Aziz^c

^aUniversité Bordeaux 1, CNRS UMR 5255, Institut des Sciences Moléculaires,
351 Cours de la Libération, Talence 33405, France

^bUMR 5258 UB1-CNRS-Solvay IPB, Laboratoire du Futur, 178 avenue Schweitzer,
Pessac 33608, France

^cUniversity of Waterloo, Department of Electrical and Computer Engineering,
200 University Avenue West, Waterloo, Ontario N2L 3G1, Canada

^dCNRS UMR 5218, Laboratoire de l'Intégration du Matériau au Système,
16 avenue Pey Berland, Pessac 33607, France

Abstract. Polymeric bulk heterojunction (BHJ) organic solar cells represent one of the most promising technologies for renewable energy with a low fabrication cost. Control over BHJ morphology is one of the key factors in obtaining high-efficiency devices. This review focuses on formulation strategies for optimizing the BHJ morphology. We address how solvent choice and the introduction of processing additives affect the morphology. We also review a number of recent studies concerning prediction methods that utilize the Hansen solubility parameters to develop efficient solvent systems. © *The Authors. Published by SPIE under a Creative Commons Attribution 3.0 Unported License. Distribution or reproduction of this work in whole or in part requires full attribution of the original publication, including its DOI.* [DOI: [10.1117/1.JPE.4.040998](https://doi.org/10.1117/1.JPE.4.040998)]

Keywords: organic photovoltaics; bulk heterojunction; formulation; processing additive; Hansen solubility parameters.

Paper 14012MV received Mar. 7, 2014; revised manuscript received Apr. 10, 2014; accepted for publication Apr. 14, 2014; published online Jun. 10, 2014.

1 Introduction

Organic solar cells (OSCs), as potential sources of renewable energy, have been the subject of much research attention. Polymeric bulk heterojunction (BHJ) OSCs are of particular interest as they have the potential to be fabricated using solution processes such as ink-jet printing and roll to roll coating.^{1,2} The use of solution processes enables the easier fabrication of large area, low cost OSCs. Consequently, a large panel of innovative devices can be considered, such as flexible, transparent, and light weight devices.^{3,4} In addition, OSC fabrication benefits from a lower energy payback time in the long term and a smaller environmental impact than other commercialized technologies.⁵ A polymeric BHJ-OSC contains a layer consisting of a multilength-scale interpenetrated network of two organic semiconducting materials: an electron donating material (D) and an electron accepting material (A). These two materials are mixed together in a solvent and coated as a thin film to form the BHJ layer. During coating, the two materials phase separate into pure domains or remain miscible. The resulting BHJ contains several phases: an A-rich domain, a D-rich domain, and an intermixed phase of D and A.⁶ The A-rich and D-rich domains can be either amorphous or crystalline.

In OSCs, the conversion of light to electricity happens in four consecutive steps: (1) light absorption and generation of excitons, (2) exciton diffusion, (3) exciton separation and charge carrier generation, and (4) transport of charge carriers to the electrodes. Because organic

*Address all correspondence to: Uyxing Vongsaysy, E-mail: uvongsay@uwaterloo.ca

semiconducting materials generally possess a large exciton binding energy (typically a few hundreds of meV),⁷ photo-generated excitons are not efficiently dissociated by ambient thermal energy. In a BHJ configuration, the chemical potential at the interface between a D and an A material enables the dissociation of excitons into free charge carriers. Hence, the exciton must be photo-generated near the interface, typically within the exciton diffusion length. When the charge carriers are generated, they require a pathway to the electrodes in order to be collected. Therefore, the morphology of the active layer is a key factor in controlling the efficiency of charge generation, charge collection, and consequently, the overall efficiency of an OSC.⁸ In the pursuit of increasing the efficiency of OSCs, much research has focused on the optimization of this morphology using various approaches. Post processing steps such as thermal annealing have proven successful in optimizing the morphology of BHJs based on D:A such as poly(3-hexylthiophene-2,5-diyl):[6,6]-phenyl-C61-butyric acid methyl ester (P3HT:PC₆₁BM).^{9,10} Despite the initial success of these techniques, such post processing steps are not fully compatible with the fabrication of large area and flexible devices, and are inefficient for some D:A systems (e.g., systems based on poly[2,6-(4,4-bis(2-ethylhexyl)-4H-cyclopenta[2,1-b;3,4-b']-dithiophene)-alt-4,7-(2,1,3-benzothiadiazole)] (PCPDTBT)).¹¹ Alternatively, the morphology of a BHJ can be controlled by tuning the solvent composition in which the D and the A are dissolved.

This work reviews some of the recent studies on addressing the effects of the solvent composition on the BHJ morphology. We begin with a brief description of the effect of the morphology on BHJ-OSCs performance. We then review work on how solvent properties influence the morphology and device characteristics. Historically, P3HT and poly[2-methoxy-5-(3-7-dimethyloctyloxy)-1,4-phenylenevinylene] (MDMO-PPV) have been the most widely used polymers at the time that solvent effects were explored. The fourth section presents an in-depth review of processing additives and their use in BHJ formulation. The first occurrence of processing additives in 2006, and the numerous reports that followed, focused not only on MDMO-PPV and P3HT blends, but also on low band gap polymers, which have been the subject of more recent studies. The final section covers some of the work addressing prediction methods for identifying efficient BHJ formulations without the need of widely used trial and error type strategies.

2 Effects of the Morphology on Efficiency

When defining the solid state morphology of a BHJ of a D:A blend, two aspects should be considered: the phase separation and the molecular organization of the components. The phase separation between the D and the A components occurring during solvent evaporation determines the sizes of the D and A domains. In order to maximize the amount of photo-generated current, the D and A domain sizes should be in the range of the exciton diffusion length. In organic semiconductors, the exciton diffusion length, which is in the range of 1 to 10 nm,¹²⁻¹⁴ dictates the domain sizes of the D and A to be around 1 to 10 nm.¹⁵ Recent findings highlighted the important role of the intermixed phase in the BHJ in the exciton quenching and charge generation processes.¹⁶⁻²⁰ In this intermixed phase, the D and the A are molecularly mixed and form amorphous domains. Studies showed that it is crucial that these intermixed phases coexist with the relatively pure D and A domains that stabilize the charge separation and enable the transport to the electrodes. In this review, we focus primarily on the phase separation between pure D and A phases that were shown to clearly influence the power conversion efficiency (PCE) of a polymeric BHJ-OSC.^{21,22} In the pursuit of acquiring an in-depth understanding of phase separation in a BHJ, various techniques have been used for characterization.^{23,24} Transmission electron microscopy (TEM) and energy filtered-TEM are useful for identifying the domains with different electron density or different elemental composition.^{25,26} Atomic force microscopy (AFM) is also commonly used to provide information on the surface topography and on the roughness of an active layer. More advanced AFM techniques such as conductive-AFM, photoconductive-AFM, and Kelvin probe microscopy provide further information on the D and A domains properties.²⁷⁻³⁰ Phase separation can also be successfully characterized using scattering techniques such as grazing incidence small angle x-ray scattering and small angle neutron scattering (SANS). All of these techniques contribute to the understanding of the relationship between the processing

history of a BHJ and the phase separation observed in the solid state. Models have been developed to explain the mechanisms driving the phase separation between a D and an A during solution deposition.³¹ However, the phase separation still remains a complex problem because it depends not only on the intrinsic properties of the D and A components such as the degree of crystallinity, their miscibility, and the self-limiting crystallization properties,³² but also—and just as importantly—on the processing conditions. In addition, the nature of the charge transport layers also influences the phase separation in the BHJ.^{33–35}

In addition to phase separation, the molecular organization within domains plays a crucial role. For polymers, the molecular organization concerns the interlayer spacing between polymer chains, the $\pi - \pi$ stacking distance, and the orientation of the polymer chains with respect to the substrate. The organization of polymer chains has been shown to greatly impact the charge carrier mobility and therefore the recombinations in OSCs.^{36,37} This can be explained by the fact that charge transport, occurring by holes hopping from chain to chain, relates exponentially to the hopping distance and thus to the interchain spacing. In OSCs, the charge carrier mobility is an important factor to optimize: both high mobility and a balance between electron and hole mobilities were shown to be beneficial.^{36,38–41} For some polymers, an increase in crystallinity is also generally accompanied by a modification in their UV–visible absorption spectra. For example, P3HT exhibits a red shift and the appearance of additional vibronic bands when the degree of crystallinity increases in the BHJ. In this case, UV–visible absorption spectroscopy can be used as a technique to characterize the crystallinity and the aggregation of polymer chains throughout the active layer. Also, x-ray diffraction (XRD), grazing incidence XRD (GIXD), and reflectivity techniques, such as high-resolution x-ray reflectivity, can be used to obtain more detailed information on the degree of crystallinity of the components, the characteristic distances between polymer chains, and their orientation.

The PCE of OSCs is clearly influenced by the morphology of the BHJ. In the following sections, we discuss how the solvent composition influences the phase separation and the molecular organization and, overall, how the solvent composition can help to achieve high efficiency OSCs.

3 Effects of the Solvent Properties in Controlling the Morphology of a BHJ

Among the commonly used solvents, chlorinated solvents such as chlorobenzene (CB), 1,2-dichlorobenzene (DCB), 1,2,4-trichlorobenzene (TCB), and chloroform (CF) are found to be good solvents for a large range of organic semiconductors. Aromatic solvents such as xylene and toluene are also commonly used. The BHJ morphology is strongly dependent on thermodynamic and kinetic aspects involved during the blend deposition.^{42,43} The thermodynamics of the system is dictated by intrinsic properties of the D and A materials (their tendency to crystallize, their interactions with each other, and their miscibility), and by the properties of the solvent [solubility, solvent:(D:A) blend interactions]. The kinetics of drying primarily depend on the boiling point and the vapor pressure of the solvent. A thorough understanding of the effects of the solubility properties and the boiling point of the solvent on the morphology are necessary in order to make a good choice of solvents for a specific D:A blend.

3.1 Effect of the Solubility Properties

Many studies have reported the effects of D and A solubility properties in a solvent on the aggregation of the fullerene derivatives (A) in the solid state. Table 1 displays the solubility limits of PC₆₁BM in some conventional solvents. The study by Brabec et al. on a blend of MDMO-PPV and PC₆₁BM was among the first to bring some insights into the relationship between D and A solubility properties in a solvent and the morphology of a BHJ.²² AFM images showed that films of MDMO–PPV:PC₆₁BM spin-cast from toluene exhibited large features that are absent from CB spin-cast films. These large features were later identified as large domains of PC₆₁BM surrounded by a polymer matrix.⁴⁴ These morphological differences were attributed to the higher solubility limit of PC₆₁BM in CB compared to that in toluene (Table 1). In CB, PC₆₁BM

Table 1 Boiling points and solubility limits of PC₆₁BM in various solvents.

Solvents	Boiling point (°C)	Solubility limit of PC ₆₁ BM (mg. mL ⁻¹)	References
Chloroform (CF)	61	25 to 26	45, 49, 55, 56
Chlorobenzene (CB)	132	25 to 59.5	45, 49, 55, 56
1,2-dichlorobenzene (ODCB)	183	42 to 107	45, 57
1,2,4-trichlorobenzene (TCB)	214	81.4	57
Toluene	112	9 to 15.6	45, 49, 55, 56
Xylene	138	5 to 22.1	45, 49, 55, 56
Mesitylene	163	47 to 48.1	55, 56
Carbon disulfide	46	207	45

molecules are more soluble and remain finely dispersed, therefore no over-sized PC₆₁BM aggregates are formed. The smoother film obtained in the case of CB led to OSC efficiencies of 2.5% which is three times higher than the efficiency of OSCs fabricated using toluene as a solvent. Figure 1 presents the AFM images from Nguyen et al. of MDMO-PPV:PC₆₁BM blends spin-cast from seven different solvents: CB, carbon disulfide, CF, pyridine, trichloroethylene, toluene, and 1-methyl pyrrole. The largest PC₆₁BM domain sizes (around 400 nm) were found in blends spin-cast from pyridine and toluene where the solubility limits were lower than in other solvents.⁴⁵ Many other studies confirmed the presence of large PC₆₁BM aggregates (up to 500 nm) in BHJ spin-cast from solvents in which PC₆₁BM has a low solubility limit.^{44–46} Similar results were reported with blends of P3HT and PC₆₁BM. In a BHJ of P3HT:PC₆₁BM, it is well known that thermal annealing causes PC₆₁BM to crystallize and to form

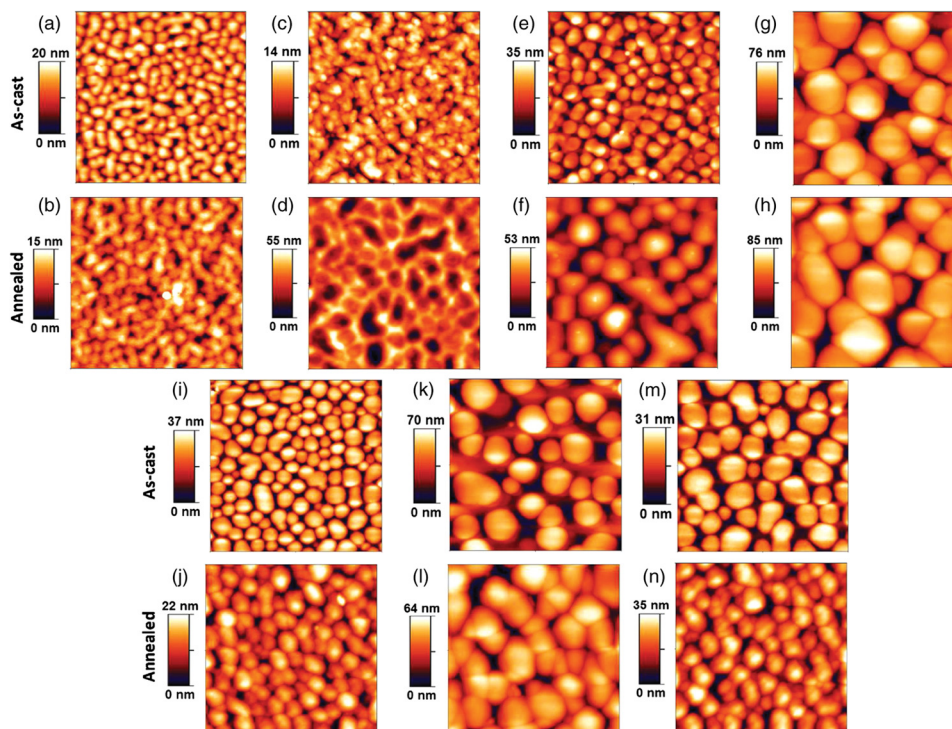


Fig. 1 Atomic force microscopy (AFM) topography images of as-cast and annealed films of MDMO-PPV-PC₆₁BM spin-cast from (a, b) chlorobenzene (CB), (c, d) carbon disulfide, (e, f) chloroform (CF), (g, h) pyridine, (i, j) trichloroethylene, (k, l) toluene, and (m, n) 1-methylpyrrole. Reproduced from Ref. 45 with permission of Wiley.

microcrystals.^{47,48} Ruderer et al. compared PC₆₁BM crystallite sizes in thermally annealed films of P3HT:PC₆₁BM spin-cast from four solvents: xylene and toluene (poor solvents for PC₆₁BM) and CB and DCB (good solvents for PC₆₁BM).⁴⁹ They showed that the BHJ presented larger PC₆₁BM microcrystals when spin-cast from poor solvents. These results suggest that for P3HT:PC₆₁BM blends as well as for MDMO-PPV:PC₆₁BM blends, the crystallization of PC₆₁BM is induced by the solubility limit of PC₆₁BM in the solvent. Troshin et al. carried out a massive study with 27 synthesized fullerene derivatives with solubility limits in CB ranging from 4 to 130 mg mL⁻¹.⁵⁰ Solution blends containing P3HT and each of the fullerene derivatives in CB were prepared and spin-cast. Optical microscopy carried out on the films showed that BHJs spin-cast using a fullerene derivative with a low solubility limit (<10 mg mL⁻¹) gave rise to large PC₆₁BM aggregates, even prior to thermal annealing. For fullerene derivatives with a solubility limit above 20 mg mL⁻¹, no aggregates were observed. Interestingly, the electrical properties of OSCs fabricated from all of these fullerene derivatives showed a nice correlation with the solubility limits (Fig. 2). The short circuit current (Jsc), the fill factor (FF), and the open circuit voltage (Voc) rapidly increased with increasing fullerene solubility from 4 to 20 mg mL⁻¹. The Jsc and FF reached maximum values when the fullerene solubility was between 20 and 40 mg mL⁻¹. Further increase in solubility led to a decrease in FF and Jsc. The authors suggested that when the PC₆₁BM solubility was too high (>40 mg mL⁻¹), PC₆₁BM molecules were intimately mixed with P3HT chains, which was detrimental for the phase separation and caused the efficiency decrease. The result of this study shows that the solubility of the fullerene component in a solvent affected the presence of aggregates in the BHJ and subsequently affected the PCE of the resulting OSC. When PC₆₁BM is blended with P3HT or MDMO-PPV, the crystallization of PC₆₁BM molecules is governed by its solubility limit. When comparing P3HT and MDMO-PPV, it is worthy to note that the crystallization of PC₆₁BM seems to depend more on solvent quality when MDMO-PPV is the donor. This divergent behavior can likely be attributed to the different strength of the interactions between the polymer and the fullerene components. Using real-time GIXD, Schmidt-Hansberg et al. showed that, in solution, P3HT and PC₆₁BM gave rise to strong Polymer-fullerene interactions

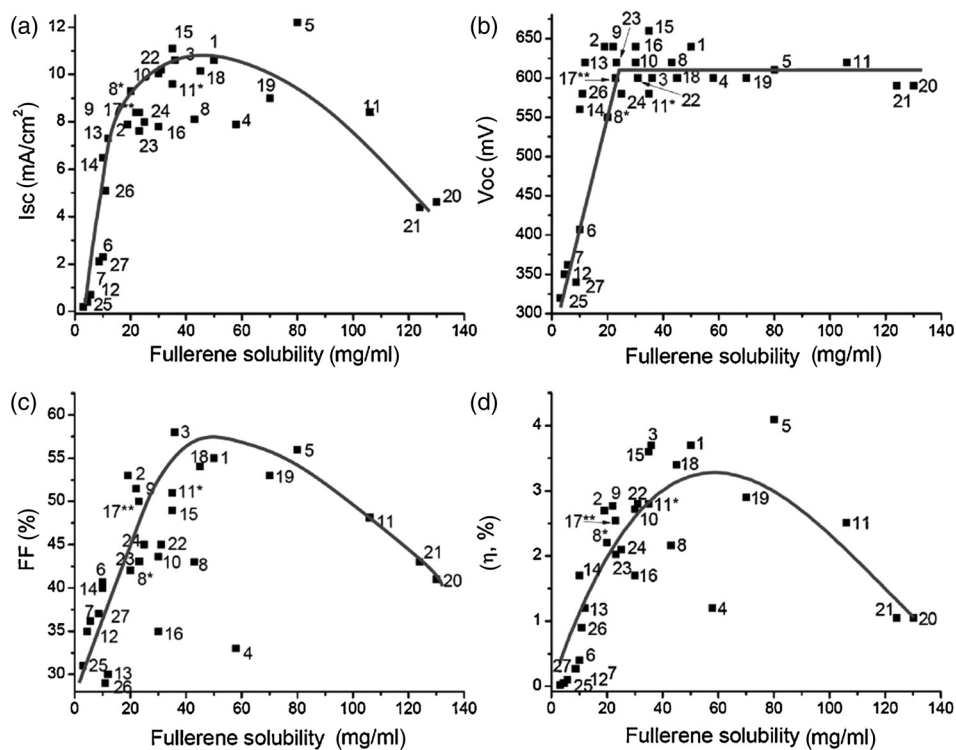


Fig. 2 Relationship between solar cell output parameters [(a) Jsc, (b) Voc, (c) FF, and (d) PCE] and solubility of the fullerene derivative used as the electron acceptor material in the active layer. Reproduced from Ref. 50 with permission of Wiley.

that delayed the aggregation of PC₆₁BM to the latest stage of the drying, long after its solubility limit was reached.⁵¹ Using MDMO-PPV or P3HT as a donor (D), the aggregation of PC₆₁BM is shown to be affected by the D-A interactions but can be tuned by the type of solvent used. D:A films containing [6,6]-phenyl C₇₁-butyric acid methyl ester (PC₇₁BM) as the acceptor were also shown to adopt morphological dependence toward the solvent used. Poly[*N*-11''-henicosanyl-2,7-carbazole-alt-5,5-(4',7'-di-2-thienyl-2',1',3'-benzothiadiazole)] (PCDTBT) is a low band gap polymer that demonstrated efficiencies up to 7.5% when blended with PC₇₁BM.⁵² AFM and TEM images of PCDTBT:PC₇₁BM films spin-cast from CB or CF showed large aggregates, which were identified as fullerene domains.^{53,54} On the other hand, films spin-cast from DCB revealed no aggregates, likely due to the higher solubility of PC₇₁BM in this solvent. The morphology obtained from DCB was shown to be beneficial for reaching high performance OSCs.

The effects of a solvent quality on the polymeric component are another important aspect to consider. On this note, it is worth examining the behavior of polymer chains alone in solution as a function of the solvent quality. It is well known that the behavior of polymer chains (the aggregation and the hydrodynamic radius) is highly dependent on the type of solvent.⁵⁸ A common method to investigate the effects of solvent quality on the behavior of P3HT chains is to add a poor solvent for the polymer (e.g., acetone, hexane) to the host solvent in order to reduce the solubility of the polymer in the solvent system. Keum et al. studied the structural evolution, in solution, of P3HT chains as a function of the solvent quality, using UV-visible absorption spectroscopy and SANS.⁵⁹ They showed that the introduction of a poor solvent caused the P3HT chains to aggregate and to grow into nanorods in order to reduce the unfavorable solvent-polymer interactions. As a consequence of the preformed aggregates in solution, the crystallinity of P3HT in the dry film greatly improved.⁶⁰ Chang et al. used GIXD to show that the introduction of acetone in the solvent system increased the crystallinity of P3HT (Fig. 3) causing as much as a 4-fold increase in mobility.⁶¹ In blends of P3HT:PC₆₁BM, the presence of preformed aggregates was also found to increase the crystallinity of P3HT in the BHJ.⁶² Moulé and Meerholz showed that the introduction of a poor solvent, nitrobenzene, caused the PCE to increase from 1.2% to 3.28% with the preformation of P3HT nanoparticles in the solution blend.⁶³ The solvent quality affects the behavior of the D and A phases: poor solvents introduce a driving force for the polymer to aggregate in order reach a thermodynamically favorable state.

3.2 Effect of Solvent's Boiling Point

The organization of the material and the transition from the liquid to the solid states can be affected by the drying kinetics. Using highly volatile solvents, the kinetics of evaporation can be much higher than the kinetics of crystallization. In that case, the resulting morphology is far from that observed under equilibrium conditions.⁵⁵ The effects of the drying kinetics on the amount of polymer chain aggregation have been widely investigated using various deposition techniques⁴³ and solvents with different boiling points. When P3HT:PC₆₁BM films were spin-cast from solvents with different boiling points, it was often observed that a high boiling point solvent leads to better efficiency on devices made without any thermal treatment.⁶⁴ Ruderer et al. studied the morphology of P3HT:PC₆₁BM films spin-cast from four different solvents (CF, CB, toluene, and xylene).³⁸ Using GIWAXS, they showed that the crystallite sizes of P3HT increased with increasing boiling point of the solvent. Similarly, Verploegen et al. showed that films spin-cast from CB gave larger crystal sizes than films spin-cast from CF.⁶⁵ This was attributed to the fact that a high boiling point solvent resulted in slow drying that provided time for the self-assembly of polymer chains during solvent evaporation. These results indicate that spin-casting from high boiling point solvents allows the P3HT component to arrange in a lower free-energy state compared with thin films spin-cast from a low boiling point solvent. This phenomenon is also observed with several other donor polymers. Fischer et al. showed that for PCPDTBT films spin-cast from low boiling point solvents such as carbon disulfide, a featureless structure was observed in AFM images.⁶⁶ When the polymer was spin-cast from a higher boiling point solvent, a fiber-like structure was obtained. For high boiling point solvents, polymer chains were given more time to organize, resulting in larger domains and higher crystallinity. Thieno[3,4-b]thiophene-alt-benzodithiophene (PTB7) similarly showed smaller domains when spin-cast from CB or CF in comparison to higher boiling point solvents (DCB).⁶⁷

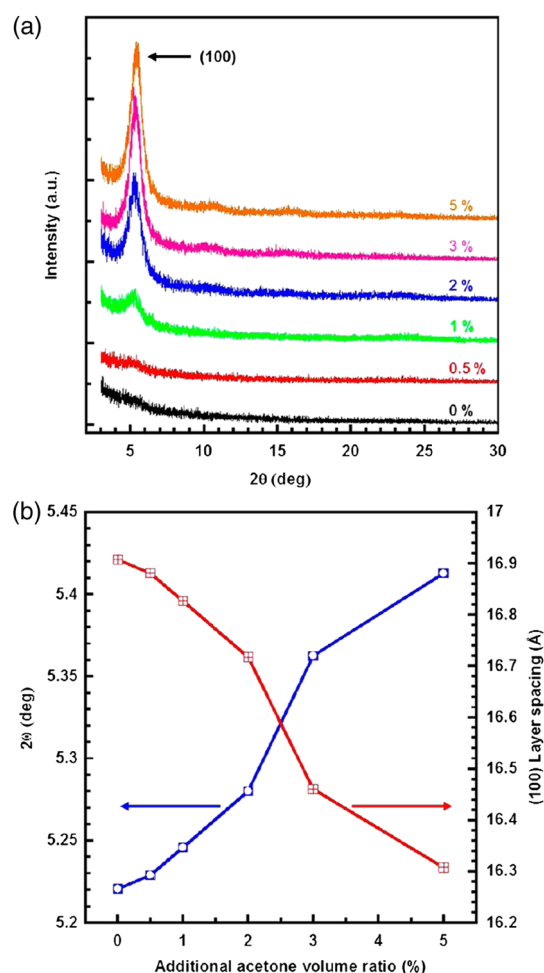


Fig. 3 (a) GIXD profiles of P3HT films spin-cast from P3HT/CF solutions containing a range of added acetone; (b) 2θ angle (left axis) of (100) peak and corresponding layer spacing (right axis) as a function of the additional acetone volume ratio. Reprinted with permission from Ref. 61. Copyright 2013, American Chemical Society.

The choice of solvents has a large impact on the morphology of the BHJ. We primarily reviewed the effects of the boiling point and the solubility on the phase separation and the crystallinity of the D:A blends. However, the choice of solvent was also shown to impact other aspects of the BHJ morphology, such as the vertical phase separation⁴⁹ and the orientation of polymer chains.⁶⁵ During solvent evaporation, the drying kinetics and thermodynamics are in competition. For P3HT:PC₆₁BM blends, high boiling point solvents are preferred to provide time for the polymer chains to self-assemble. An appropriate choice of solvent can, therefore, optimize the morphology of a BHJ. However, a limited number of solvents are available that can solubilize both D and A components. Other alternatives are therefore needed to fine-tune the morphology at the formulation level. For this reason, processing additives can provide a complementary way to control the morphology.

4 Effects of Processing Additives

A processing additive—also called a solvent additive—refers to a solvent which is introduced in small proportion (generally a few volume %) into the host solvent used to solubilize the active materials. In their pioneering work on processing additives, Peet et al. showed that introducing 1,8-octanedithiol (ODT) significantly increased the photocurrent and the PCE of OSCs using P3HT or PCPDTBT as the donor material.^{11,68} Following the processing additives approach, other solvents were found to increase the PCE of OSCs: alkanedithiol with various alkane

chain lengths,^{11,69,70} 1,8-diiodooctane (DIO),^{71,72} 1-chloronaphthalene (CN),^{73–76} and 1,8-dichloro-octane.^{71,77} Processing additives have been the subject of increasing interest because they contribute to the optimization of the active layer morphology of a wide range of polymeric and molecular BHJs and consequently, in increasing the efficiency of the resulting OSCs.^{78,79} For the archetypical system P3HT:PC₆₁BM, processing additives could be used to reach efficiencies normally obtained with postprocessing steps such as thermal annealing.^{69,80} This is particularly appealing for the prospect of low fabrication cost. More importantly, processing additives were found to be effective in increasing the PCE of polymeric BHJ-OSCs for which postprocessing steps were unsuccessful.⁵⁴ Early investigation on the properties of processing additives suggested that they should possess (i) a good solubility toward the fullerene derivative acceptor, (ii) a poor solubility toward the polymer, and (iii) a boiling point higher than the host solvent.⁷¹ These criteria have been widely accepted by the community to explain the mechanistic effects of processing additives on the BHJ formation. The presence of processing additives in the solvent blend introduces further interactions in addition to the solvent-polymer and solvent-fullerene interactions, since processing additives interfere in the phase separation and crystallization by selectively dissolving the fullerene component. As a consequence, processing additives induce remarkable morphological change in the BHJ that will be highlighted in this section. Beforehand, we want to stress that CN is a processing additive that does not follow the above criteria.^{76,81} Its effect on morphology will be treated separately from the others.

Table 2 displays the effects of the processing additives for various D:A blends. We can observe that their effects vary with the type of D:A blend under investigation, e.g., in some cases they can increase the phase separation whereas in other cases they decrease it. An example of a system for which processing additives are used to reduce the phase separation is the blend using PCPDTBT as the donor. PCPDTBT is a low band gap copolymer that was found to form a finely mixed interpenetrated network with fullerene derivatives when spin-cast from a pure solvent. When no processing additive was used, spin-cast blends from PCPDTBT presented a finely mixed interpenetrated network where the fullerene component and the polymer chains were finely dispersed.^{77,82} This configuration was attributed to the high miscibility of the fullerene component with the polymer chains, which prevents the polymer from aggregating. In order to investigate the effect of the miscibility of the fullerene component and the polymer chains, Gu et al. conducted GIXD characterization.⁷⁷ The diffraction patterns of pure PCPDTBT showed diffraction peaks characteristic for PCPDTBT packing that disappeared in the diffraction pattern of a blend of PCPDTBT and PC₇₁BM. This result demonstrated that the presence of PC₇₁BM caused a disruption in PCPDTBT packing. Similar studies carried out with GIWAXS also showed a disruption of the polymer packing when PC₇₁BM was introduced in the solution blend.⁸² Consequently, a finely mixed morphology could be formed as can be observed from the TEM images from Liao et al. depicted in Fig. 4.³⁰ On the contrary, TEM images of blends spin-cast from a solution mixture containing a processing additive showed spherical-like domains of polymer which formed a phase separated system with PC₆₁BM, in contrast with the featureless morphology obtained when no processing additive was used. Several other contributions also showed the increased phase separation upon the introduction of processing additives with TEM,^{71,83} as well as AFM images.^{11,71,72,84} With the aim of investigating the mechanisms behind the effects of the processing additives on the formation of larger phase separation, Peet et al. investigated the evolution of the aggregates of PCPDTBT during solvent evaporation using UV-visible spectroscopy⁸⁵ [Fig. 5(a)]. They showed that introducing DIO in the solvent blend enabled the aggregation of PCPDTBT chains before total evaporation of the solvent, causing the aggregation of the polymer to occur in a fluid medium in which the polymer chains were mobile. Additionally, Gu et al. suggested that the aggregation of polymer chains in solution happened without the disruption of PC₆₁BM due to the solubility properties of DIO, which caused an increase in phase separation as depicted in Fig. 5(b).⁷⁷ The introduction of processing additives raised the PCE of OSCs from 3.5% up to 5.5% with an alkanedithiol^{11,82} and up to 5.12% with DIO.^{71,77,83} Processing additives were also found to increase the aggregation and crystallinity of other D:A systems such as P3HT:PC₆₁BM for which efficiencies up to 4.03% could be reached upon their use.^{69,70,80}

Table 2 Effects of processing additives on the phase separation of various D:A blends and the efficiency of OSCs based on them.

D:A blend	Additives	Phase separation	Efficiency without-additive	References
P3HT:PC ₆₁ BM	1,8-octanedithiol	Increase	0.6% to 2.6%	80
P3HT:PC ₆₁ BM	1,6-hexanedithiol	Increase	0.46% to 3.16%	70
P3HT:ICBA ^a	<i>N</i> -methyl-2-pyrrolydinone	Decrease	1.15% to 3.45%	86
	1,8-diiiodooctane		1.15% to 2.97%	
	1,8-octanedithiol		1.15% to 3.09%	
PCDTBT ^b :PC ₇₁ BM	1,8-diiiodooctane	Increase	4.89% to 5.91%	72
PCPDTBT:PC ₇₁ BM	Alkanedithiol	Increase	2.8% to 5.5%	11
	Alkanedithiol	Increase	No PCE reported	82, 84, 87
PCPDTBT:PC ₇₁ BM	1,8-diiiodooctane	Increase	2.6% to 4.5%	83
	1,8-diiiodooctane	Increase	No PCE reported	81
PCPDTBT:PC ₇₁ BM	1,8-octanedithiol	Increase	3.35% to 4.50%	71
	1,8-diiiodooctane		3.35% to 5.12%	
	1,8-dibromooctane		3.35% to 4.66%	
PCPDTBT:PC ₆₁ BM	1,8-diiiodooctane	Increase	1.68% to 4.62%	77
	1,8-octanedithiol		1.68% to 3.87%	
	1,8-dichlorooctane		1.68% to 3.45%	
PTB7:PC ₇₁ BM	1,8-diiiodooctane	Decrease	3.92% to 7.40%	88
	1,8-diiiodooctane	Decrease	No PCE reported	89
DPPT ^c :PC ₆₁ BM	1,8-diiiodooctane	Decrease	0.6% to 3.4%	90
DPPBT ^d :PC ₆₁ BM	1,8-diiiodooctane	Decrease	1.0% to 5.2%	90
PDTSTPD:PC ₇₁ BM	1,8-diiiodooctane	Decrease	1.0% to 7.3%	91, 92

^aIndene-C60 bisadduct.

^bPoly[*N*-11''-henicosanyl-2,7-carbazole-alt-5,5-(4',7'-di-2-thienyl-2',1',3'-benzothiadiazole)].

^cPoly(diketopyrrolopyrrole-terthio-phenylene).

^dPoly(diketopyrrolopyrrole-quaterthio-phenylene).

As mentioned above, processing additives can also decrease the phase separation for certain types of D:A systems. An example of a donor material for which processing additives reduce the phase separation is PTB7. PTB7 is an excellent polymer when used in OSCs and can lead to high efficiencies up to 9.2%.⁹³ Contrary to PCPDTBT, BHJs based on PTB7 spin-cast from a solution without processing additive demonstrate significant phase separation primarily due to aggregation of the fullerene component into extended domain sizes. The introduction of processing additives in the solution blend can reduce the phase separation by preventing the aggregation of PC₇₁BM. This hypothesis was supported by the work of Lou et al. who used SAXS to characterize blends of PTB7 and PC₇₁BM.⁸⁹ The scattering profile of a blend of PTB7:PC₇₁BM spin-cast using DIO showed that the PC₇₁BM peak had a lower intensity compared with the PC₇₁BM peak in a blend spin-cast without processing additives [Fig. 6(A)]. This suggested that fewer PC₇₁BM aggregates were present in the BHJ spin-cast using DIO. Interestingly, the peak of PTB7 did not show significant differences. This observation confirmed that the introduction of DIO primarily impacted the aggregation of the fullerene component. Also, TEM

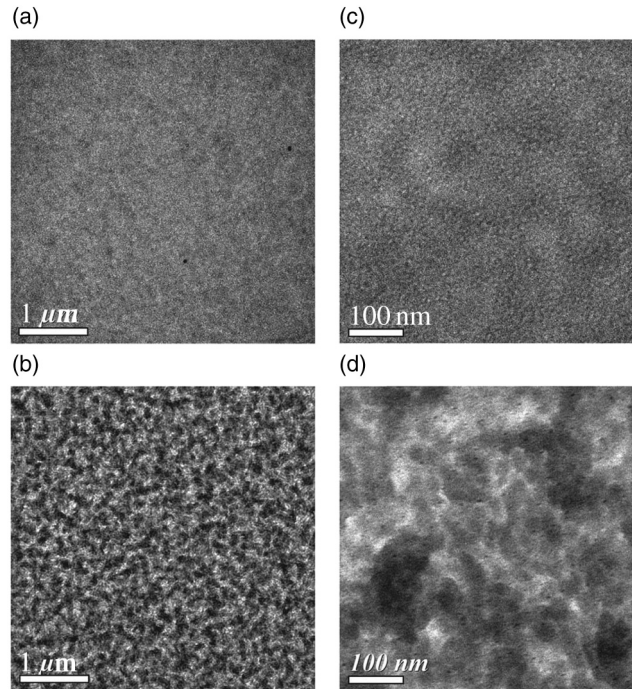


Fig. 4 Transmission electron microscopy (TEM) images of pristine PCPDTBT films processed without (a and c), and with 3%DIO (b and d), respectively. Reproduced from Ref. 30 with permission of The Royal Society of Chemistry.

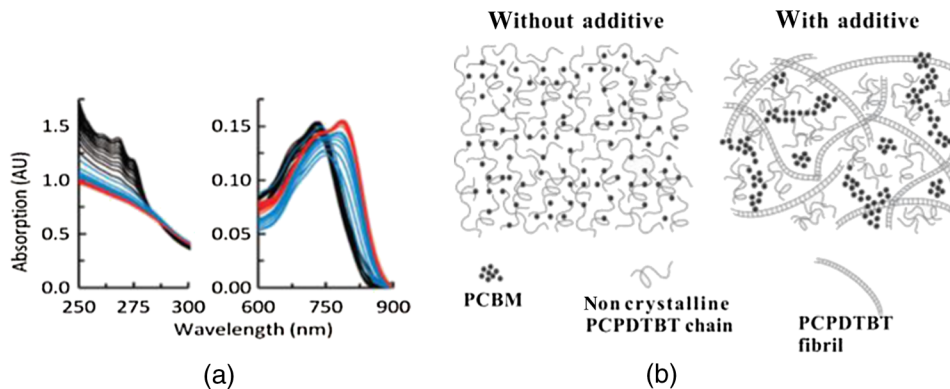


Fig. 5 (a) Absorption spectra as a function of time after spin-casting for 10 s at 2000 rpm from TCB with 2% DIO in 90-s intervals (black and blue) and then 10-min intervals (red). Reprinted with permission from Ref. 85. Copyright 2008, American Chemical Society. (b) Morphology for PCPDTBT:PC₆₁BM thin films processed both without and with additives. Reproduced from Ref. 77 with permission of Wiley.

images showed that the large aggregates present in films spin-cast from pure solvent disappeared in films spin-cast in the presence of DIO (Fig. 7).²⁶ Without DIO, the aggregates could have a particularly wide size distribution—from 20 to 100 nm. They were reduced to 20 to 40 nm with the use of DIO.²⁶ Clearly, the presence of DIO reduced the aggregation of PC₇₁BM. In order to explain this effect, the authors suggested that DIO kept the fullerene component dissolved in the solution and therefore allowed it to mix well with the polymer chains. Subsequently, the aggregation of the fullerene component into large domains was inhibited. This mechanism is illustrated in Fig. 6(B). The optimized phase separation leads to significant improvement in the PCE, for example, Liang et al. showed that the introduction of DIO could raise the PCE from 3.92% to 7.40%.⁸⁸

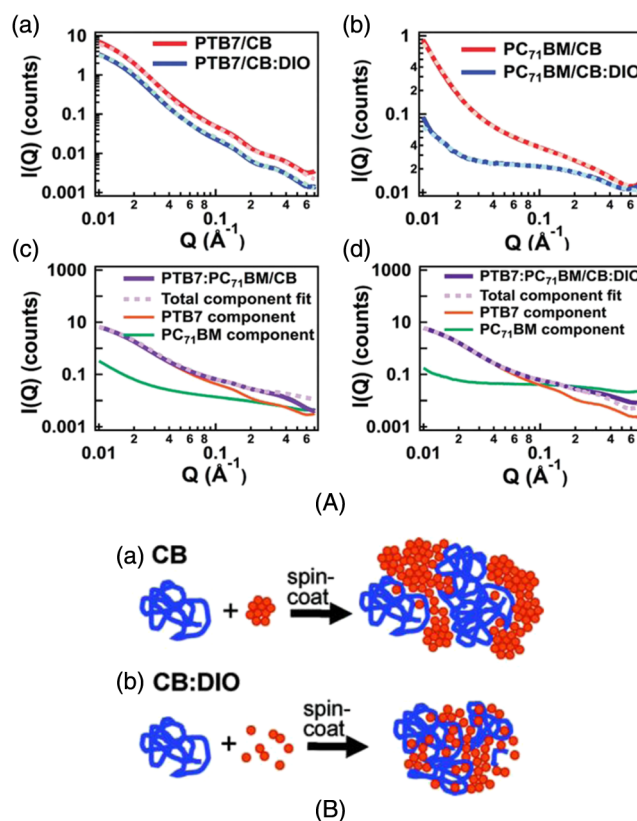


Fig. 6 (A) Experimental scattering profiles of solutions of the active layer (solid lines) and fits (dotted lines), comparing aggregation in CB and CB:DIO solutions of (a) PTB7 (offset) and (b) PC_{71}BM , and two-component fits of PTB7: PC_{71}BM in (c) CB and (d) CB:DIO. (B) Scheme showing the morphology obtained with or without DIO. Reprinted with permission from Ref. 89. Copyright 2011, American Chemical Society.

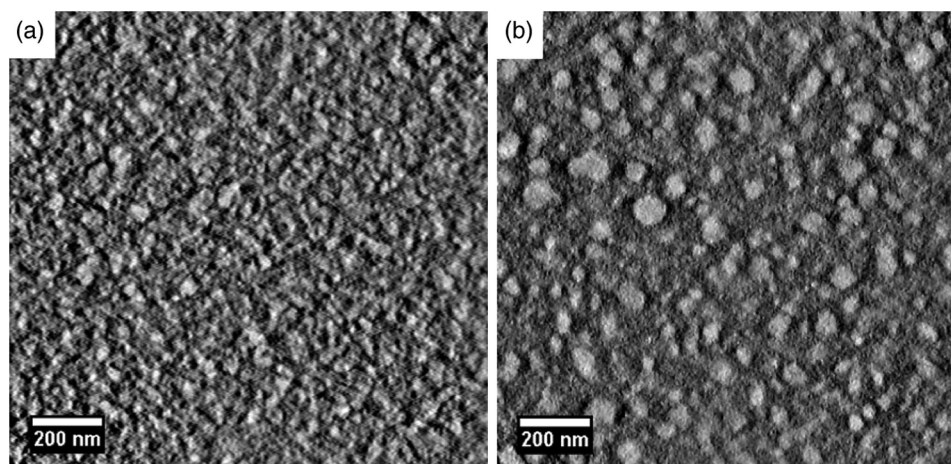


Fig. 7 Results from energy filtered-TEM tomography reconstructions of (a) the blend of PTB7: PC_{71}BM film cast from DCB/DIO and (b) the blend of PTB7: PC_{71}BM cast from DCB only. PC_{71}BM -rich regions appear bright in these images. Reprinted with permission from Ref. 26. Copyright 2011, American Chemical Society.

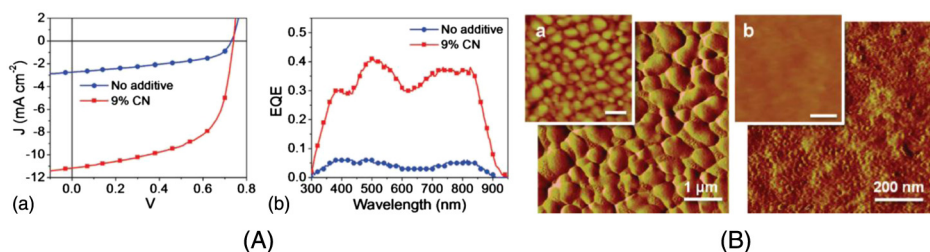


Fig. 8 (A) External quantum efficiency spectra of optimized PDPP2FT:PC₇₁BM devices spin-cast out of CB (with no additive and with 9 vol. % CN). (B) AFM images of PDPP2FT:PC₇₁BM blend films spin-cast (a) from CB only and (b) from CB + 9 vol. % CN. Reprinted with permission from Ref. 95. Copyright 2010, American Chemical Society.

4.1 Case of CN

CN is another material that has been used as a processing additive,^{94,95} but unlike other processing additives such as DIO or ODT, CN is a good solvent for the fullerene derivative (e.g., the solubility of PC₇₁BM in CN was reported to be above 400 mg mL⁻¹)⁸¹ and is known for being a good solvent for aromatic polymers.^{76,81} Kim et al. showed that adding CN to a blend with a quinoxaline-based polymer led to an increase in PCE, unlike what occurred when adding ODT and DIO.⁹⁶ Also, Woo et al. reported that the introduction of CN in a blend solution containing a furan and DPP based low band gap polymer (PDPP2FT) significantly increased the external quantum efficiency (EQE) [Fig. 8(A)] and raised the efficiency from 0.86% to 4.7%.⁹⁵ The authors attributed the improvement of the electrical parameters with the introduction of CN to decreased phase separation as depicted in the AFM images in Fig. 8(B). Other groups have also reported the role of CN as an agent in reducing phase separation. For the quinoxaline based polymer, Kim et al. suggested that CN improved the intercalation of PC₇₁BM within the polymer which prevented PC₇₁BM from forming large aggregates. This was accompanied with a decrease in electron mobility by an order of magnitude that brought the ratio of hole mobility to electron mobility from 2.66 to 1.11. The balance of charge mobility and the decreased phase separation caused a dramatic increase in the EQE and the J_{sc}, raising the overall efficiency from 3.61% to 7.08%. Using TEM, Moon et al. confirmed the effects of CN on decreasing PC₇₁BM domain size on a blend of poly[(4,4-didodecyldithieno[3,2-b:20,30-d]silole)-2,6-diyl-alt-(2,1,3-benzothiadiazole)-4,7-diyl] (Si-PDTBT) and PC₇₁BM.⁷⁵ Their TEM images, depicted in Fig. 9, demonstrated that crystallites of over 200 nm were suppressed by adding CN.

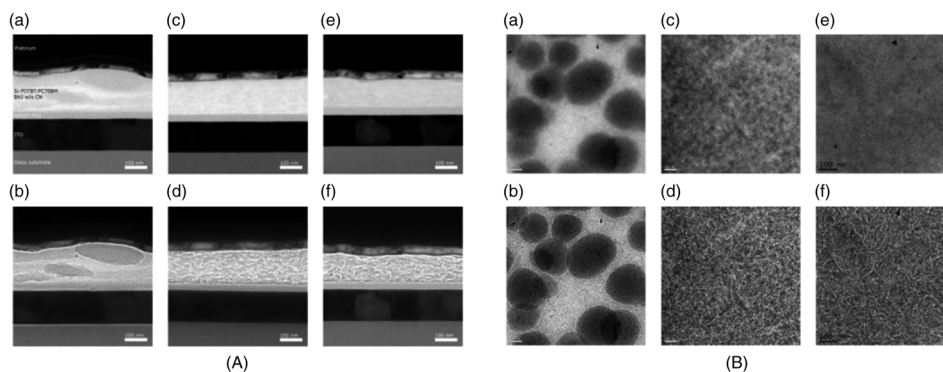


Fig. 9 (A) TEM cross-section images of Si-PDTBT:PC₇₁BM BHJ spin-cast from CB solution with and without using CN: (a) in-focus w/o CN additive, (b) -25 μm defocus w/o CN additive, (c) in-focus w/1% CN additive, (d) -25 μm defocus w/1% CN additive, (e) in-focus w/4% CN additive, and (f) -25 μm defocus w/4% CN additive. (B) TEM top-down images of Si-PDTBT:PC₇₁BM BHJ: (a) in-focus w/o CN additive, (b) -25 μm defocus w/o CN additive, (c) in-focus w/1% CN additive, (d) -25 μm defocus w/1% CN additive, (e) in-focus w/4% CN additive, and (f) -25 μm defocus w/4% CN additive. Reprinted with permission from Ref. 75. Copyright 2010, American Chemical Society.

In other D:A blends, CN was found to reduce the aggregation of polymers. This effect is observed for blends of poly(benzo[1,2-b:4,5-b']dithiophene-alt-thieno[3,4-c]pyrrole-4,6-dione) (PBDTTPD) and PC₆₁BM⁶¹ or blends of poly[(4,4-didodecyldithieno[3,2-b:2',0']silole)-2,6-diyl-alt-(2,1,3-benzoxadiazole)-4,7-diyl] and PC₇₁BM.⁸¹ CN was reported to control the aggregation of polymers that have a strong tendency to crystallize by enhancing the solubility of the polymer, and thereby suppressing the formation of large domains.^{76,81,91} Aïch et al. reported that the introduction of CN in a blend PBDTTPD and PC₆₁BM suppressed the aggregation of the polymer chains and raised the PCE of OSCs from 2.7% to 4.7%. Interestingly, they also combined CN and DIO to create a coadditive system where the CN had the role of controlling the aggregation of the polymer while DIO could selectively dissolve PC₆₁BM and thereby control the aggregation of PC₆₁BM. By combining 4% CN and 1% DIO, an impressive PCE of 7.1% was achieved. They also demonstrated another coadditive system based on methyl naphthalene and DIO to control the polymer and the PC₆₁BM aggregation.⁹¹

5 Predictive Methods for Optimizing the BHJ Morphology

The above discussion shows that the formulation plays a crucial role in defining the morphology of the active layers. The D:A BHJ morphology can be optimized by appropriate choice of solvents, solvent blends, and processing additives. Additionally, the solid content and the ratio of D to A also contribute in modifying the morphology of a BHJ.^{97–99} Considering all of these parameters and the large variety of solvents and processing additives in existence, optimizing the active layer morphology using a trial and error method involves the formulation of many material blends and the fabrication of many OSCs. Consequently, optimization of the morphology can be extremely expensive and time consuming. There is therefore a need to find novel methods for identifying efficient formulations. In that context, different strategies have been considered. The group of Krebs developed a roll-to-roll fabrication process enabling the deposition of active layers with a gradient of D and A ratios and solvent concentrations.^{46,100,101} This method could rapidly identify the optimal solid content and the optimal D to A ratio. Also, a method using the Hansen solubility theory has emerged to help select solvents and processing additives for the formulation of D:A blends. The Hansen solubility theory uses the Hansen solubility parameters (HSPs) to describe the interactions that a compound or a solute can create. HSPs are widely used to determine solvents in the coating industry,¹⁰² but emerged only recently in the field of organic electronics as a tool to predict the solubility properties of the active materials. HSPs correspond to a set of three parameters: δ_d , δ_p , and δ_h that describe the three major types of interactions in common organic materials: (i) dispersion interactions, (ii) permanent dipole–permanent dipole molecular interactions, and (iii) hydrogen bonding interactions. The units of these parameters are MPa^{1/2}. Every chemical compound can be graphically represented by its position in a three-dimensional space, the Hansen solubility space, with coordinates defined by the three solubility parameters. Comparing the HSPs of a solute and a solvent provides insight into whether interactions between them are favorable or not: if the HSPs are similar enough, the solvent is considered to be a good solvent for the solute. Such similarity is quantified by the distance R_A between the HSPs of the solvent δ_{D1} , δ_{P1} , and δ_{H1} and the HSPs of the solute δ_{D2} , δ_{P2} , and δ_{H2} . The distance R_A is calculated using the following equation:

$$R_A^2 = 4(\delta_{D1} - \delta_{D2})^2 + (\delta_{P1} - \delta_{P2})^2 + (\delta_{H1} - \delta_{H2})^2. \quad (1)$$

In addition to δ_{D2} , δ_{P2} and δ_{H2} , a solute requires a boundary of solubility to define and differentiate between “sufficient” and “nonsufficient” interactions from a solubility standpoint. Therefore, a solute is described as a sphere in the Hansen solubility space, the HSPs are the coordinates of the center of the sphere, and R_O is the radius representing the boundary of solubility. The interactions between a solvent and a solute are considered to be strong only if the distance R_A is smaller than the radius of the sphere R_O . In order to compare R_A and R_O , the relative energy difference (RED) can be calculated using the following equation:

$$\text{RED} = \frac{R_A}{R_O}. \quad (2)$$

If the RED is higher than 1, the solute is expected to be a bad solvent, while if the RED is between 0 and 1, the solvent is expected to be a good solvent. The HSPs of a wide range of solvents can be found in reference textbooks.¹⁰² In 2011, Machui et al. determined the HSPs of three organic semi-conductors, P3HT, PC₆₁BM, and PCPDTBT, by performing solubility tests.⁵⁷ The method using solubility tests generally consists of blending the materials of interest in various distinct solvents (Machui et al. used 34 solvents in their study). The solubility of the material in each of the solvents can be visually assessed and categorized as either a good or a bad solvent. These results are used to fit the solubility sphere of the material where all good solvents are inside the sphere, and bad solvents are outside the sphere. The three coordinates of the center of the sphere correspond to the HSPs of the compound. The determination of the HSPs are dependent on the experimental parameters, such as the number of solvents involved in the solubility tests, the solid content, and the method used to differentiate good and bad solvents. In 2012, Machui et al. introduced a binary gradient blend method for the more accurate determination of the HSPs, especially at the boundary of the sphere.⁵⁶ Nguyen's group used UV-visible absorption spectroscopy to differentiate good and bad solvents.^{45,103} The group contribution approach can also be used. This method predicts the HSPs of a compound by adding the solubility parameters of all contributing chemical groups. Table 3 displays the values of HSPs found in the literature for P3HT, PC₆₁BM, and PC₇₁BM, and the method used to determine them. We present the values of the most widely used materials, but the HSPs of

Table 3 Hansen solubility parameters of P3HT, PC₆₁BM, and PC₇₁BM and the methods used to determine them.

Material	δ_D (MPa ^{1/2})	δ_P (MPa ^{1/2})	δ_H (MPa ^{1/2})	R_O (MPa ^{1/2})	Methods (tests—number of solvents—method for the determination of solubility—concentration limit)	References
P3HT	18.5	5.3	5.3	2.7	Solubility tests—34 solvents—visual inspection—2.5 mg mL ⁻¹	57
	18.3	3.9	0.3	2.6	Solubility tests—binary gradient blends—2 mg mL ⁻¹	56
	18.56	2.88	3.19	3.6	Solubility tests—27 solvents—UV-visible absorption—various concentration limit	45
	19.05	3.3	2.8	3.9	Solubility tests—54 solvents and 10 solvent mixtures—visual inspection—2 mg mL ⁻¹	107
PC ₆₁ BM	20.4	3.5	7.2	7.5	Solubility tests—34 solvents—visual inspection—2.5 mg mL ⁻¹	57
	19.7	7.4	6.6	5.8	Solubility tests—gradient binary blends—2 mg mL ⁻¹	56
	20.6	2.4	3.5		Group contribution method	63
	19.89	5.68	3.64	6.6	Solubility tests—27 solvents—UV-visible absorption—various concentration limit	34
	20.02	5.2	5.88	8.4	Solubility tests—54 solvents and 10 solvent mixtures—visual inspection—2 mg mL ⁻¹	107
PC ₇₁ BM	20.16	5.37	4.49	7	Solubility tests—27 solvents—UV-visible absorption—various concentration limit	45
	19.82	6.6	6.82	6.8	Solubility tests—3 binary gradient blends—2 mg mL ⁻¹	56
	20.16	5.37	6.26		Solubility tests—29 solvents—UV-visible absorption	103

other materials can be found elsewhere in Refs. 45 and 57. The determination of the HSPs enables the rational design of a solvent system for processing the active materials.^{103,104} Machui et al. used the HSPs to study the effects on the OSC efficiencies of introducing a bad solvent (acetone) into a good host solvent (CB).⁵⁶ The HSP calculations predicted that a solvent mixture of 30% acetone in CB remained a good solvent for P3HT and PC₆₁BM whereas a further increase in acetone concentration led to a nonsolubilizing mixture. OSCs fabricated using a solvent mixture containing 30% acetone had efficiencies similar to OSCs fabricated from pure CB (2.7% and 2.9%, respectively). On the other hand, solvent systems containing 40% of acetone and characterized as a nonsolubilizing mixture from the HSPs calculation could not be processed. This shows that the HSPs are able to predict the boundary between good and bad solvents, which determines whether or not a certain formulation is processable. HSPs were also used to find substitutes for conventional solvents. This was proven interesting in two cases. First, conventional solvents are not always appropriate for spin-casting certain types of D:A blends. Cho et al. found that the blend of PC₇₁BM and an indacenodithiophene-based ladder-type donor polymer spin-cast from the conventional DCB led to a small phase separation. Solubility parameters were used to design a blend of solvents consisting of DCB and tetrahydrofuran (THF) that had a selective solubility and could enhance the aggregation of PC₇₁BM.¹⁰⁵ The blend of 30% THF in DCB led to a PCE of 6.9% compared with 6.2% when the film was spin-cast from a pure solvent. Second, conventional solvents are halogenated and in most cases not appropriate for large area coating because of health risks. Therefore, it is of great interest to substitute for them with nonhalogenated solvents. Park et al. used a blend of solvents with similar HSPs to DCB to process a blend of P3HT and PC₆₁BM.¹⁰⁴ They were successful in finding a blend of mesitylene and acetophenone that could act as substitutes to DCB. A blend of mesitylene and acetophenone in an 80/20 proportion achieved PCEs similar to those obtained from pure ODCB (3.38% and 3.92%, respectively). More recently, the method of using the HSPs to find nonhalogenated solvents were extended to small molecular based BHJs.¹⁰⁶ Burgués-Ceballos et al. used this approach to replace CB as a host solvent for a blend of tris{4-[5''-(1,1-dicyanobut-1-en-2-yl)-2,2'-bithiophen-5-yl]phenyl}amine and PC₇₁BM. The HSPs helped in identifying two environmentally friendly solvent systems: benzaldehyde and a mixture of benzaldehyde and mesitylene. The OSCs obtained from these two solvent systems had PCEs of 3.6% and 3.7%, respectively, which were similar to the PCEs of OSCs obtained from pure CB (3.34%). Finally, the HSPs were also used to predict efficient processing additives. Our group recently identified selection rules based on the HSPs to identify appropriate processing additives for a blend based on P3HT and PC₆₁BM.¹⁰⁷ Based on the requirement that efficient processing additives should be a good solvent for PC₆₁BM and a bad solvent for P3HT, we defined selection criteria rules that needed to be satisfied by a processing additive as follows: RED with P3HT > 1.0 and RED with PC₆₁BM < 0.9. Additionally, the processing additive should have a high boiling point. Applying these selection criteria to a list of over 700 solvents, three novel efficient processing additives were selected and demonstrated to be efficient in increasing the efficiency of OSCs. This contribution showed that the HSPs represent a tool that could help identify processing additives appropriate for a specific type of D and A blends. Graham et al. investigated the effects of processing additives on BHJ based on a thiophene/isoindigo small molecule as the donor and PC₆₁BM as the acceptor.⁷⁹ The HSPs were used to correlate the effects of the solubility properties of processing additives on the morphology of a molecular BHJ and on the efficiencies of OSCs. AFM and TEM images showed that when the blend was spin-cast using processing additives with a low solubility toward the two compounds (<0.8 mg mL⁻¹), small features were observed. For processing additives that better solubilized the two materials (small molecule and PC₆₁BM solubility >0.9 and >30 mg mL⁻¹, respectively) the observed feature sizes were larger. Processing additives with a low solubility toward the materials tended to increase the efficiency. This study provided a correlation between the solubility properties of the processing additives and their effects on the morphology and the efficiencies. Altogether, the HSPs appear to be a useful tool for the prediction of efficient processing additives and for predicting their effects as a function of their solubility properties.

6 Conclusion

In this review, we examined the impacts of various solvent components and their formulation on the morphology of the active light-harvesting layers and the electrical parameters of OSCs based on them. First, we discussed the effects of the solubility properties and their boiling points, then gave an overview of the effect of introducing processing additives on the formulation. Processing additives were shown to provide an additional means of controlling phase separation and the molecular ordering of the D:A components. Finally, we introduced the use of the HSPs as a predictive tool to guide the selection of solvents and processing additives. The use of HSPs proved to be useful in guiding the formulation of D:A blends or predicting the BHJ morphology. The large body of research focused on optimizing and characterizing BHJ morphology has advanced our understanding of the interplay between processing conditions and morphology. With the goal of further increasing efficiency, but also of bringing laboratory scale coating to industrial scale production, studies on the effects of formulation on morphology will continue to play a key role.

Acknowledgments

The authors would like to acknowledge financial support to this work from the Natural Sciences and Engineering Research Council of Canada. U.V. acknowledges financial support through Waterloo Institute for Nanotechnology Nanofellowship.

References

1. F. C. Krebs, "Fabrication and processing of polymer solar cells: a review of printing and coating techniques," *Sol. Energy Mater. Sol. Cells* **93**(4), 394–412 (2009), <http://dx.doi.org/10.1016/j.solmat.2008.10.004>.
2. F. C. Krebs, J. Fyenbo, and M. Jorgensen, "Product integration of compact roll-to-roll processed polymer solar cell modules: methods and manufacture using flexographic printing, slot-die coating and rotary screen printing," *J. Mater. Chem.* **20**(41), 8994–9001 (2010), <http://dx.doi.org/10.1039/c0jm01178a>.
3. R. R. Sondergaard, M. Hösel, and F. C. Krebs, "Roll-to-roll fabrication of large area functional organic materials," *J. Polym. Sci., Part B: Polym. Phys.* **51**(1), 16–34 (2013), <http://dx.doi.org/10.1002/polb.v51.1>.
4. C.-C. Chen et al., "Visibly transparent polymer solar cells produced by solution processing," *ACS Nano* **6**(8), 7185–7190 (2012), <http://dx.doi.org/10.1021/nm3029327>.
5. S. B. Darling and F. You, "The case for organic photovoltaics," *RSC Adv.* **3**(39), 17633–17648 (2013), <http://dx.doi.org/10.1039/c3ra42989j>.
6. B. A. Collins et al., "Molecular miscibility of polymer-fullerene blends," *J. Phys. Chem. Lett.* **1**(21), 3160–3166 (2010), <http://dx.doi.org/10.1021/jz101276h>.
7. S. F. Alvarado et al., "Direct determination of the exciton binding energy of conjugated polymers using a scanning tunneling microscope," *Phys. Rev. Lett.* **81**(5), 1082–1085 (1998), <http://dx.doi.org/10.1103/PhysRevLett.81.1082>.
8. W. A. Hammed et al., "Recent approaches to controlling the nanoscale morphology of polymer-based bulk-heterojunction solar cells," *Energies* **6**(11), 5847–5868 (2013), <http://dx.doi.org/10.3390/en6115847>.
9. D. Chen et al., "P3HT/PCBM bulk heterojunction organic photovoltaics: correlating efficiency and morphology," *Nano Lett.* **11**(2), 561–567 (2011), <http://dx.doi.org/10.1021/nl103482n>.
10. F.-C. Chen et al., "Morphological study of P3HT:PCBM blend films prepared through solvent annealing for solar cell applications," *Sol. Energy Mater. Sol. Cells* **94**(12), 2426–2430 (2010), <http://dx.doi.org/10.1016/j.solmat.2010.09.004>.
11. J. Peet et al., "Efficiency enhancement in low-bandgap polymer solar cells by processing with alkane dithiols," *Nat. Mater.* **6**(7), 497–500 (2007), <http://dx.doi.org/10.1038/nmat1928>.

12. J. J. M. Halls et al., "Exciton diffusion and dissociation in a poly(p-phenylenevinylene)/C60 heterojunction photovoltaic cell," *Appl. Phys. Lett.* **68**(22), 3120–3122 (1996), <http://dx.doi.org/10.1063/1.115797>.
13. T. Stübinger and W. Brütting, "Exciton diffusion and optical interference in organic donor-acceptor photovoltaic cells," *J. Appl. Phys.* **90**(7), 3632–3641 (2001), <http://dx.doi.org/10.1063/1.1394920>.
14. D. E. Markov et al., "Dynamics of exciton diffusion in poly(p-phenylene vinylene)/fullerene heterostructures," *Phys. Rev. B* **72**(4), 045217 (2005), <http://dx.doi.org/10.1103/PhysRevB.72.045217>.
15. S. Günes, H. Neugebauer, and N. S. Sariciftci, "Conjugated polymer-based organic solar cells," *Chem. Rev.* **107**(4), 1324–1338 (2007), <http://dx.doi.org/10.1021/cr050149z>.
16. J. A. Bartelt et al., "The importance of fullerene percolation in the mixed regions of polymer-fullerene bulk heterojunction solar cells," *Adv. Energy Mater.* **3**(3), 364–374 (2013), <http://dx.doi.org/10.1002/aenm.v3.3>.
17. S. Shoaee et al., "Charge photogeneration for a series of thiazolo-thiazole donor polymers blended with the fullerene electron acceptors PCBM and ICBA," *Adv. Funct. Mater.* **23**(26), 3286–3298 (2013), <http://dx.doi.org/10.1002/adfm.v23.26>.
18. P. Westacott et al., "On the role of intermixed phases in organic photovoltaic blends," *Energy Environ. Sci.* **6**(9), 2756–2764 (2013), <http://dx.doi.org/10.1039/c3ee41821a>.
19. W. Chen et al., "Hierarchical nanomorphologies promote exciton dissociation in polymer/fullerene bulk heterojunction solar cells," *Nano Lett.* **11**(9), 3707–3713 (2011), <http://dx.doi.org/10.1021/nl201715q>.
20. N. D. Treat et al., "Polymer-fullerene miscibility: a metric for screening new materials for high-performance organic solar cells," *J. Am. Chem. Soc.* **134**(38), 15869–15879 (2012), <http://dx.doi.org/10.1021/ja305875u>.
21. M. T. Rispens et al., "Influence of the solvent on the crystal structure of PCBM and the efficiency of MDMO-PPV:PCBM 'plastic' solar cells," *Chem. Commun.* (17), 2116–2118 (2003), <http://dx.doi.org/10.1039/b305988j>.
22. S. E. Shaheen et al., "2.5% efficient organic plastic solar cells," *Appl. Phys. Lett.* **78**(6), 841–843 (2001), <http://dx.doi.org/10.1063/1.1345834>.
23. F. Liu et al., "Characterization of the morphology of solution-processed bulk heterojunction organic photovoltaics," *Prog. Polym. Sci.* **38**(12), 1990–2052 (2013), <http://dx.doi.org/10.1016/j.progpolymsci.2013.07.010>.
24. W. Chen, M. P. Nikiforov, and S. B. Darling, "Morphology characterization in organic and hybrid solar cells," *Energy Environ. Sci.* **5**(8), 8045–8074 (2012), <http://dx.doi.org/10.1039/c2ee22056c>.
25. S. D. Oosterhout et al., "The effect of three-dimensional morphology on the efficiency of hybrid polymer solar cells," *Nat. Mater.* **8**(10), 818–824 (2009), <http://dx.doi.org/10.1038/nmat2533>.
26. M. R. Hammond et al., "Molecular order in high-efficiency polymer/fullerene bulk heterojunction solar cells," *ACS Nano* **5**(10), 8248–8257 (2011), <http://dx.doi.org/10.1021/nn202951e>.
27. J. Sun et al., "Nanoscale imaging of dense fiber morphology and local electrical response in conductive regioregular poly(3-hexylthiophene)," *Org. Electron.* **15**(2), 441–448 (2014), <http://dx.doi.org/10.1016/j.orgel.2013.11.032>.
28. G. J. Hedley et al., "Determining the optimum morphology in high-performance Polymer-fullerene organic photovoltaic cells," *Nat. Commun.* **4**, 1–10 (2013), <http://dx.doi.org/10.1038/ncomms3867>.
29. L. Kaake et al., "Effects of impurities on operational mechanism of organic bulk heterojunction solar cells," *Adv. Mater.* **25**(12), 1706–1712 (2013), <http://dx.doi.org/10.1002/adma.v25.12>.
30. H.-C. Liao et al., "Bi-hierarchical nanostructures of donor-acceptor copolymer and fullerene for high efficient bulk heterojunction solar cells," *Energy Environ. Sci.* **6**(6), 1938–1948 (2013), <http://dx.doi.org/10.1039/c3ee24312e>.
31. S. Kouijzer et al., "Predicting morphologies of solution processed polymer:fullerene blends," *J. Am. Chem. Soc.* **135**(32), 12057–12067 (2013), <http://dx.doi.org/10.1021/ja405493j>.

32. M. J. Sobkowicz et al., "Effect of fullerenes on crystallization-induced aggregation in polymer photovoltaics casting solutions," *Macromolecules* **45**(2), 1046–1055 (2012), <http://dx.doi.org/10.1021/ma202083q>.
33. M. Campoy-Quiles et al., "Morphology evolution via self-organization and lateral and vertical diffusion in polymer:fullerene solar cell blends," *Nat. Mater.* **7**(2), 158–164 (2008), <http://dx.doi.org/10.1038/nmat2102>.
34. T.-H. Lai et al., "Properties of interlayer for organic photovoltaics," *Mater. Today* **16**(11), 424–432 (2013), <http://dx.doi.org/10.1016/j.mattod.2013.10.001>.
35. J. R. Manders et al., "Solution-processed nickel oxide hole transport layers in high efficiency polymer photovoltaic cells," *Adv. Funct. Mater.* **23**(23), 2993–3001 (2013), <http://dx.doi.org/10.1002/adfm.v23.23>.
36. O. Oklobia and T. S. Shafai, "Correlation between charge carriers mobility and nanomorphology in a blend of P3HT/PCBM bulk heterojunction solar cell: impact on recombination mechanisms," *Sol. Energy Mater. Sol. Cells* **122**, 158–163 (2014), <http://dx.doi.org/10.1016/j.solmat.2013.11.035>.
37. J. H. Park et al., "Enhanced device performance of organic solar cells via reduction of the crystallinity in the donor polymer," *J. Mat. Chem.* **20**(28), 5860–5865 (2010), <http://dx.doi.org/10.1039/c0jm00664e>.
38. C.-T. Lee and C.-H. Lee, "Conversion efficiency improvement mechanisms of polymer solar cells by balance electron–hole mobility using blended P3HT:PCBM:pentacene active layer," *Org. Electron.* **14**(8), 2046–2050 (2013), <http://dx.doi.org/10.1016/j.orgel.2013.04.038>.
39. J. D. Kotlarski, D. J. D. Moet, and P. W. M. Blom, "Role of balanced charge carrier transport in low band gap polymer: fullerene bulk heterojunction solar cells," *J. Polym. Sci., Part B: Polym. Phys.* **49**(10), 708–711 (2011), <http://dx.doi.org/10.1002/polb.22243>.
40. M. Abbas and N. Tekin, "Balanced charge carrier mobilities in bulk heterojunction organic solar cells," *Appl. Phys. Lett.* **101**(7), 073302 (2012), <http://dx.doi.org/10.1063/1.4745602>.
41. M.-C. Chen et al., "Improving the efficiency of an organic solar cell by a polymer additive to optimize the charge carriers mobility," *Appl. Phys. Lett.* **99**(22), 223305 (2011), <http://dx.doi.org/10.1063/1.3664127>.
42. R. Mens et al., "Influence of the processing solvent on the photoactive layer nanomorphology of P3HT/PC60BM solar cells," *J. Polym. Sci., Part A: Polym. Chem.* **50**(6), 1037–1041 (2012), <http://dx.doi.org/10.1002/pola.v50.5>.
43. X. Yang et al., "Crystalline organization of a methanofullerene as used for plastic solar-cell applications," *Adv. Mater.* **16**(910), 802–806 (2004), [http://dx.doi.org/10.1002/\(ISSN\)1521-4095](http://dx.doi.org/10.1002/(ISSN)1521-4095).
44. H. Hoppe et al., "Efficiency limiting morphological factors of MDMO-PPV:PCBM plastic solar cells," *Thin Solid Films* **511–512**, 587–592 (2006), <http://dx.doi.org/10.1016/j.tsf.2005.12.071>.
45. D. T. Duong et al., "Molecular solubility and Hansen solubility parameters for the analysis of phase separation in bulk heterojunctions," *J. Polym. Sci., Part B: Polym. Phys.* **50**(20), 1405–1413 (2012), <http://dx.doi.org/10.1002/polb.v50.20>.
46. H. Hoppe et al., "Nanoscale morphology of conjugated polymer/fullerene-based bulk-heterojunction solar cells," *Adv. Funct. Mater.* **14**(10), 1005–1011 (2004), [http://dx.doi.org/10.1002/\(ISSN\)1616-3028](http://dx.doi.org/10.1002/(ISSN)1616-3028).
47. D. E. Motaung et al., "Comparative study: the effect of annealing conditions on the properties of P3HT:PCBM blends," *J. Mater. Sci.* **48**(4), 1763–1778 (2013), <http://dx.doi.org/10.1007/s10853-012-6937-6>.
48. L. Chang et al., "Effect of trace solvent on the morphology of P3HT:PCBM bulk heterojunction solar cells," *Adv. Funct. Mater.* **21**(10), 1779–1787 (2011), <http://dx.doi.org/10.1002/adfm.201002372>.
49. M. A. Ruderer et al., "Solvent-induced morphology in polymer-based systems for organic photovoltaics," *Adv. Funct. Mater.* **21**(17), 3382–3391 (2011), <http://dx.doi.org/10.1002/adfm.201100945>.
50. P. A. Troshin et al., "Material solubility-photovoltaic performance relationship in the design of novel fullerene derivatives for bulk heterojunction solar cells," *Adv. Funct. Mater.* **19**(5), 779–788 (2009), <http://dx.doi.org/10.1002/adfm.v19:5>.

51. B. Schmidt-Hansberg et al., "Moving through the phase diagram: morphology formation in solution cast Polymer-fullerene blend films for organic solar cells," *ACS Nano* **5**(11), 8579–8590 (2011), <http://dx.doi.org/10.1021/nn2036279>.
52. S. Beaupré and M. Leclerc, "PCDTBT: en route for low cost plastic solar cells," *J. Mater. Chem. A* **1**(37), 11097–11105 (2013), <http://dx.doi.org/10.1039/c3ta12420g>.
53. P.-K. Shin et al., "Effects of organic solvents for composite active layer of PCDTBT/PC71BM on characteristics of organic solar cell devices," *Int. J. Photoenergy* **2014**, 1–8 (2014), <http://dx.doi.org/10.1155/2014/786468>.
54. S. H. Park et al., "Bulk heterojunction solar cells with internal quantum efficiency approaching 100%," *Nat. Photonics* **3**(5), 297–302 (2009), <http://dx.doi.org/10.1038/nphoton.2009.69>.
55. S. Nilsson et al., "Morphology and phase segregation of spin-casted films of polyfluorene/PCBM blends," *Macromolecules* **40**(23), 8291–8301 (2007), <http://dx.doi.org/10.1021/ma070712a>.
56. F. Machui et al., "Determination of the P3HT:PCBM solubility parameters via a binary solvent gradient method: impact of solubility on the photovoltaic performance," *Sol. Energy Mater. Sol. Cells* **100**, 138–146 (2012), <http://dx.doi.org/10.1016/j.solmat.2012.01.005>.
57. F. Machui et al., "Determination of solubility parameters for organic semiconductor formulations," *Macromol. Chem. Phys.* **212**(19), 2159–2165 (2011), <http://dx.doi.org/10.1002/macp.v212.19>.
58. D. Wang et al., "From single chains to aggregates, how conjugated polymers behave in dilute solutions," *Macromolecules* **46**(15), 6217–6224 (2013), <http://dx.doi.org/10.1021/ma4011523>.
59. K. Keum et al., "Solvent quality-induced nucleation and growth of parallelepiped nanorods in dilute poly(3-hexylthiophene) (P3HT) solution and the impact on the crystalline morphology of solution-cast thin film," *CrystEngComm* **15**(6), 1114–1124 (2013), <http://dx.doi.org/10.1039/c2ce26666k>.
60. C. Scharsich et al., "Control of aggregate formation in poly(3-hexylthiophene) by solvent, molecular weight, and synthetic method," *J. Polym. Sci., Part B: Polym. Phys.* **50**(6), 442–453 (2012), <http://dx.doi.org/10.1002/polb.v50.6>.
61. M. Chang et al., "Solvent based hydrogen bonding: impact on poly (3-hexylthiophene) nanoscale morphology and charge," *ACS Nano* **7**(6), 5402–5413 (2013), <http://dx.doi.org/10.1021/nn401323f>.
62. S. Berson et al., "Poly(3-hexylthiophene) fibers for photovoltaic applications," *Adv. Funct. Mater.* **17**(8), 1377–1384 (2007), [http://dx.doi.org/10.1002/\(ISSN\)1616-3028](http://dx.doi.org/10.1002/(ISSN)1616-3028).
63. A. J. Moulé and K. Meerholz, "Controlling morphology in Polymer-fullerene mixtures," *Adv. Mater.* **20**(2), 240–245 (2008), [http://dx.doi.org/10.1002/\(ISSN\)1521-4095](http://dx.doi.org/10.1002/(ISSN)1521-4095).
64. M. T. Dang et al., "Polymeric solar cells based on P3HT:PCBM: role of the casting solvent," *Sol. Energy Mater. Sol. Cells* **95**(12), 3408–3418 (2011), <http://dx.doi.org/10.1016/j.solmat.2011.07.039>.
65. E. Verploegen et al., "Manipulating the morphology of P3HT-PCBM bulk heterojunction blends with solvent vapor annealing," *Chem. Mater.* **24**(20), 3923–3931 (2012), <http://dx.doi.org/10.1021/cm302312a>.
66. F. S. U. Fischer et al., "Influence of processing solvents on optical properties and morphology of a semicrystalline low bandgap polymer in the neutral and charged states," *Macromolecules* **46**(12), 4924–4931 (2013), <http://dx.doi.org/10.1021/ma400939z>.
67. S. Guo et al., "Influence of solvent and solvent additive on the morphology of PTB7 films probed via x-ray scattering," *J. Phys. Chem. B* **118**(344), 344–350 (2014), <http://dx.doi.org/10.1021/jp410075a>.
68. J. Peet et al., "Method for increasing the photoconductive response in conjugated polymer/fullerene composites," *Appl. Phys. Lett.* **89**(25), 252105 (2006), <http://dx.doi.org/10.1063/1.2408661>.
69. J. Ouyang and Y. Xia, "High-performance polymer photovoltaic cells with thick P3HT:PCBM films prepared by a quick drying process," *Sol. Energy Mater. Sol. Cells* **93**(9), 1592–1597 (2009), <http://dx.doi.org/10.1016/j.solmat.2009.04.015>.

70. T. Salim et al., "Solvent additives and their effects on blend morphologies of bulk heterojunctions," *J. Mater. Chem.* **21**(1), 242–250 (2011), <http://dx.doi.org/10.1039/c0jm01976c>.
71. J. K. Lee et al., "Processing additives for improved efficiency from bulk heterojunction solar cells," *J. Am. Chem. Soc.* **130**(11), 3619–3623 (2008), <http://dx.doi.org/10.1021/ja710079w>.
72. Z. Liu, H. Ju, and E.-C. Lee, "Improvement of polycarbazole-based organic bulk-heterojunction solar cells using 1,8-diodooctane," *Appl. Phys. Lett.* **103**(13), 133308 (2013), <http://dx.doi.org/10.1063/1.4823582>.
73. J. Jo et al., "Bulk heterojunction solar cells based on a low-bandgap carbazole-diketopyrrolopyrrole copolymer," *Appl. Phys. Lett.* **97**(20), 203303 (2010), <http://dx.doi.org/10.1063/1.3508951>.
74. T. K. An et al., "Solvent additive to achieve highly ordered nanostructural semicrystalline DPP copolymers: toward a high charge carrier mobility," *Adv. Mater.* **25**(48), 7003–7009 (2013), <http://dx.doi.org/10.1002/adma.v25.48>.
75. J. S. Moon et al., "Effect of processing additive on the nanomorphology of a bulk heterojunction material," *Nano Lett.* **10**(10), 4005–4008 (2010), <http://dx.doi.org/10.1021/nl101923m>.
76. B. R. Aich et al., "Control of the active layer nanomorphology by using co-additives towards high-performance bulk heterojunction solar cells," *Org. Electron.* **13**(9), 1736–1741 (2012), <http://dx.doi.org/10.1016/j.orgel.2012.05.001>.
77. Y. Gu, C. Wang, and T. P. Russell, "Multi-length-scale morphologies in PCPDTBT/PCBM bulk-heterojunction solar cells," *Adv. Energy Mater.* **2**(6), 683–690 (2012), <http://dx.doi.org/10.1002/aenm.201100726>.
78. H.-C. Liao et al., "Additives for morphology control in high-efficiency organic solar cells," *Mater. Today* **16**(9), 326–336 (2013), <http://dx.doi.org/10.1016/j.mattod.2013.08.013>.
79. K. R. Graham et al., "Improved performance of molecular bulk-heterojunction photovoltaic cells through predictable selection of solvent additives," *Adv. Funct. Mater.* **22**(22), 4801–4813 (2012), <http://dx.doi.org/10.1002/adfm.v22.22>.
80. H.-Y. Chen et al., "Fast-grown interpenetrating network in poly(3-hexylthiophene): methanofullerenes solar cells processed with additive," *J. Phys. Chem. C* **113**(18), 7946–7953 (2009), <http://dx.doi.org/10.1021/jp810798z>.
81. C. V. Hoven et al., "Improved performance of polymer bulk heterojunction solar cells through the reduction of phase separation via solvent additives," *Adv. Mater.* **22**(8), E63–E66 (2010), <http://dx.doi.org/10.1002/adma.v22:8>.
82. J. T. Rogers et al., "Structural order in bulk heterojunction films prepared with solvent additives," *Adv. Mater.* **23**(20), 2284–2288 (2011), <http://dx.doi.org/10.1002/adma.201003690>.
83. S. Albrecht et al., "On the field dependence of free charge carrier generation and recombination in blends of PCPDTBT/PC70BM: influence of solvent additives," *J. Phys. Chem.* **3**(5), 640–645 (2012), <http://dx.doi.org/10.1021/jz3000849>.
84. M. Dante, A. Garcia, and T.-Q. Nguyen, "Three-dimensional nanoscale organization of highly efficient low band-gap conjugated polymer bulk heterojunction solar cells," *J. Phys. Chem. C* **113**(4), 1596–1600 (2009), <http://dx.doi.org/10.1021/jp809650p>.
85. J. Peet et al., "Transition from solution to the solid state in polymer solar cells cast from mixed solvents," *Macromolecules* **41**(22), 8655–8659 (2008), <http://dx.doi.org/10.1021/ma801945h>.
86. X. Guo et al., "High efficiency polymer solar cells based on poly(3-hexylthiophene)/indene-C70 bisadduct with solvent additive," *Energy Environ. Sci.* **5**(7), 7943–7949 (2012), <http://dx.doi.org/10.1039/c2ee21481d>.
87. T. Agostinelli et al., "The role of alkane dithiols in controlling polymer crystallization in small band gap polymer:fullerene solar cells," *J. Polym. Sci., Part B: Polym. Phys.* **49**(10), 717–724 (2011), <http://dx.doi.org/10.1002/polb.22244>.
88. Y. Liang et al., "For the bright future-bulk heterojunction polymer solar cells with power conversion efficiency of 7.4%," *Adv. Mater.* **22**(20), E135–E138 (2010), <http://dx.doi.org/10.1002/adma.200903528>.

89. S. J. Lou et al., "Effects of additives on the morphology of solution phase aggregates formed by active layer components of high-efficiency organic solar cells," *J. Am. Chem. Soc.* **133**(51), 20661–20663 (2011), <http://dx.doi.org/10.1021/ja2085564>.
90. F. Liu et al., "Relating chemical structure to device performance via morphology control in diketopyrrolopyrrole-based low band gap polymers," *J. Am. Chem. Soc.* **135**(51), 19248–19259 (2013), <http://dx.doi.org/10.1021/ja408923y>.
91. B. R. Aich et al., "Highly efficient thieno[3,4-c]pyrrole-4,6-dione-based solar cells processed from non-chlorinated solvent," *Org. Electron.* **15**(2), 543–548 (2014), <http://dx.doi.org/10.1016/j.orgel.2013.12.012>.
92. T.-Y. Chu et al., "Bulk heterojunction solar cells using thieno[3,4-c]pyrrole-4,6-dione and dithieno[3,2-b:2',3'-d]silole copolymer with a power conversion efficiency of 7.3%," *J. Am. Chem. Soc.* **133**(12), 4250–4253 (2011), <http://dx.doi.org/10.1021/ja200314m>.
93. Z. He et al., "Enhanced power-conversion efficiency in polymer solar cells using an inverted device structure," *Nat. Photonics* **6**(9), 591–595 (2012), <http://dx.doi.org/10.1038/nphoton.2012.190>.
94. H.-Y. Chen et al., "Morphologic improvement of the PBDTTT-C and PC71BM blend film with mixed solvent for high-performance inverted polymer solar cells," *Nanotechnology* **24**(48), 484009 (2013), <http://dx.doi.org/10.1088/0957-4484/24/48/484009>.
95. C. H. Woo et al., "Incorporation of furan into low band-gap polymers for efficient solar cells," *J. Am. Chem. Soc.* **132**(44), 15547–15549 (2010), <http://dx.doi.org/10.1021/ja108115y>.
96. Y. Kim et al., "High-efficiency polymer solar cells with a cost-effective quinoxaline polymer through nanoscale morphology control induced by practical processing additives," *Energy Environ.* **6**(6), 1909–1916 (2013), <http://dx.doi.org/10.1039/c3ee00110e>.
97. H. Park et al., "Discrepancy of optimum ratio in bulk heterojunction photovoltaic devices: initial cell efficiency vs long-term stability," *ACS Appl. Mater. Interfaces* **5**(5), 1612–1618 (2013), <http://dx.doi.org/10.1021/am302185f>.
98. M. T. Dang et al., "Controlling the morphology and performance of bulk heterojunctions in solar cells. lessons learned from the benchmark system," *Chem. Rev.* **113**(5), 3734–3765 (2013), <http://dx.doi.org/10.1021/cr300005u>.
99. W.-H. Baek et al., "Effect of P3HT:PCBM concentration in solvent on performances of organic solar cells," *Sol. Energy Mater. Sol. Cells* **93**(8), 1263–1267 (2009), <http://dx.doi.org/10.1016/j.solmat.2009.01.019>.
100. H. F. Dam and F. C. Krebs, "Simple roll coater with variable coating and temperature control for printed polymer solar cells," *Sol. Energy Mater. Sol. Cells* **97**, 191–196 (2012), <http://dx.doi.org/10.1016/j.solmat.2011.08.027>.
101. J. Alstrup et al., "Ultra fast and parsimonious materials screening for polymer solar cells using differentially pumped slot-die coating," *ACS Appl. Mater. Interfaces* **2**(10), 2819–2827 (2010), <http://dx.doi.org/10.1021/am100505e>.
102. C. M. Hansen, *Hansen Solubility Parameters: A User's Handbook*, 2nd Ed., Taylor & Francis Group, Boca Raton, FL (2007).
103. B. Walker et al., "A systematic approach to solvent selection based on cohesive energy densities in a molecular bulk heterojunction system," *Adv. Energy Mater.* **1**(2), 221–229 (2011), <http://dx.doi.org/10.1002/aenm.201000054>.
104. C.-D. Park et al., "High performance bulk-heterojunction organic solar cells fabricated with non-halogenated solvent processing," *Org. Electron.* **12**(9), 1465–1470 (2011), <http://dx.doi.org/10.1016/j.orgel.2011.05.020>.
105. N. Cho, H.-L. Yip, and A. K.-Y. Jen, "Morphology evolution by controlling solvent-solute interactions using a binary solvent in bulk heterojunction solar cells," *Appl. Phys. Lett.* **102**(23), 233903 (2013), <http://dx.doi.org/10.1063/1.4811173>.
106. I. Burgués-Ceballos et al., "Solubility based identification of green solvents for small molecule organic solar cells," *Adv. Funct. Mater.* **24**(10), 1449–1457 (2013), <http://dx.doi.org/10.1002/adfm.201301509>.
107. U. Vongsaysy et al., "Guiding the selection of processing additives for increasing the efficiency of bulk heterojunction polymeric solar cells," *Adv. Energy Mater.* **4**(3) (2013), <http://dx.doi.org/10.1002/aenm.201300752>.

Uyxing Vongsaysy is currently a PhD student in a collaborative program between the University of Bordeaux in France and the University of Waterloo in Canada. She received her Master of Science from the University of Bordeaux in 2010. Her research interests include the control and the characterization of the bulk heterojunction morphology in organic solar cells.

Dario M. Bassani is a senior scientist at the CNRS Institute of Molecular Science at the University of Bordeaux. He received his PhD in organic photochemistry from Northwestern University in 1993 and conducts research focused on supramolecular photochemistry and molecular electronics. He is the co-author of over 80 research articles and received the 2005 Grammaticakis-Neumann prize from the Swiss Chemical Society.

Laurent Servant is a professor in chemistry at the University of Bordeaux. His main research interests are in the application of optical spectroscopies techniques to the investigation of chemical problems (e.g. electrochemistry; interfaces; energy storage devices, microfluidics).

Bertrand Pavageau joined the chemical company Rhodia (now Solvay) in 1995 at the research centre of Aubervilliers. He was in charge of the analytical development for the characterization of polymers. In 2005, he moved to Bordeaux and since 2010, he is a senior scientist at the head of a multicultural team. He is in charge of projects related to energy such as batteries, heat storage, bioenergy, and organic electronics.

Guillaume Wantz is associate professor in the laboratory IMS at the University of Bordeaux, France, since 2006. His research interest is in organic electronics with a focus on polymer photovoltaic solar cells and light-emitting electrochemical cells. His research deals with device fabrication and optimization through careful control of nanoscale morphologies and the development of original device architectures. He is currently developing strategies to improve the stability of polymer bulk heterojunctions for long-lived solar cells.

Hany Aziz is a professor in the Department of Electrical and Computer Engineering, University of Waterloo, Canada. His research interests are in the area of organic electronic and optoelectronic materials and devices. He has published more than 100 papers and holds 51 US patents. He received a PhD in Materials Science and Engineering from McMaster University in 1999. He was a research scientist at Xerox Research Centre of Canada in the period 1999–2007.